Interactive CardioVascular and Thoracic Surgery 20 (2015) 200–208
doi:10.1093/icvts/ivu357 Advance Access publication 31 October 2014

Four-dimensional modelling of the mitral valve by real-time 3D transoesophageal echocardiography: proof of concept†

Thilo Noack[a,*], Chirojit Mukherjee[b], Philipp Kiefer[a], Fabian Emrich[a], Marcel Vollroth[a], Razvan Ioan Ionasec[c], Ingmar Voigt[c], Helene Houle[d], Joerg Ender[b], Martin Misfeld[a], Friedrich Wilhelm Mohr[a] and Joerg Seeburger[a]

[a] Department of Cardiac Surgery, Heart Center Leipzig University, Leipzig, Germany
[b] Department of Anesthesia, Heart Center Leipzig University, Leipzig, Germany
[c] Image Analytics and Informatics, Siemens Corporate Research, Princeton, NJ, USA
[d] Ultrasound Division, Siemens Healthcare, Mountain View, CA, USA

* Corresponding author. Department of Cardiac Surgery, Heart Center, Leipzig University, 04289 Leipzig, Germany. Tel: +49-341-8651421; fax: +49-341-8651452; e-mail: thilo.noack@medizin.uni-leipzig.de (T. Noack).

Received 28 July 2014; accepted 19 September 2014

Abstract

OBJECTIVES: The complexity of the mitral valve (MV) anatomy and function is not yet fully understood. Assessing the dynamic movement and interaction of MV components to define MV physiology during the complete cardiac cycle remains a challenge. We herein describe a novel semi-automated 4D MV model.

METHODS: The model applies quantitative analysis of the MV over a complete cardiac cycle based on real-time 3D transoesophageal echocardiography (RT3DE) data. RT3DE data of MVs were acquired for 18 patients. The MV annulus and leaflets were semi-automatically reconstructed. Dimensions of the mitral annulus (anteroposterior and anterolateral–posteromedial diameter, annular circumference, annular area) and leaflets (MV orifice area, intercommissural distance) were acquired. Variability and reproducibility (intraclass correlation coefficient, ICC) for interobserver and intraobserver comparison were quantified at 4 time points during the cardiac cycle (mid-systole, end-systole, mid-diastole and end-diastole).

RESULTS: Mitral annular dimensions provided highly reliable and reproducible measurements throughout the cardiac cycle for interobserver (variability range, 0.5–1.5%; ICC range, 0.895–0.987) and intraobserver (variability range, 0.5–1.6%; ICC range, 0.827–0.980) comparison, respectively. MV leaflet parameters showed a high reliability in the diastolic phase (variability range, 0.6–9.1%; ICC range, 0.750–0.986), whereas MV leaflet dimensions showed a high variability and lower correlation in the systolic phase (variability range, 0.6–22.4%; ICC range, 0.446–0.915) compared with the diastolic phase.

CONCLUSIONS: This 4D model provides detailed morphological reconstruction as well as sophisticated quantification of the complex MV structure and dynamics throughout the cardiac cycle with a precision not yet described.

Keywords: Echocardiography • Mitral valve • 4D reconstruction • Model

INTRODUCTION

Substantial progress in surgical and percutaneous treatment of structural mitral valve (MV) disease has reinforced the interest in non-invasive quantitative analyses of MV morphology and function [1, 2].

With the advances of real-time 3D transoesophageal echocardiography (RT3DE) and the introduction of RT3DE-based comprehensive MV reconstructions, improved quantification and characterization of the MV has been realized [3–5]. Multiple studies show the feasibility of RT3DE-based MV models to accurately assess the MV apparatus [6–10]. However, the existing models are limited by static measurements at a predefined phase of the cardiac cycle without inclusion of any motion. These measurements are time-consuming and hence difficult to integrate into clinical practice [9, 11].

We herein present a novel semi-automated RT3DE-based 4D MV model, which allows a comprehensive quantitative analysis of MV annulus and leaflets during the entire cardiac cycle. Model specifications, reproducibility by inter- and intraobserver variability and 4D visualization are reported and discussed.

MATERIALS AND METHODS

Patients

In surgical patients with isolated coronary artery diseases (CADs) who underwent coronary artery bypass graft surgery, a clinically indicated RT3DE [12] was performed after induction of general anaesthesia and endotracheal intubation but prior to surgery. Exclusion criteria for RT3DE were (i) contraindication to transoesophageal echocardiography, (ii) the presence of MV disease (regurgitation

† Presented at the 27th Annual Meeting of the European Association for Cardio-Thoracic Surgery, Vienna, Austria, 5–9 October 2013.

and/or stenosis graded higher than grade 1+) and (iii) concomitant cardiac valve disease (aortic, pulmonary and tricuspid valve). Written informed consent was obtained from each individual patient.

Echocardiography

RT3DE was performed using an iE33 ultrasound system equipped with an X7-2t transoesophageal echocardiography matrix transducer (both Philips Deutschland GmbH, Hamburg). Electrocardiographically (ECG)-gated full-volume and 3D zoom data sets for the MV were acquired over four cardiac cycles at a frame rate of 10–30 frames per second (Fig. 1A). All examinations in this study were performed by two certified cardiac anaesthesiologists (according to the European Association of Cardiovascular Imaging). Preoperative transthoracic 2D echocardiography determined left ventricular ejection fraction, end-diastolic volume and end-systolic volume. A standard examination protocol was used for all examinations.

Image segmentation and mitral valve modelling

RT3DE data were analysed using specifically designed software (eSie Valves^{TM}, Siemens Medical Solutions, USA). Besides image visualization and interactive navigation functionality, the software includes a workflow comprising automated MV segmentation, fast interactive model validation and model-based 2D and 3D measurements throughout the cardiac cycle [see items (i) to (iv)]. The automated segmentation is based on an algorithm, which has been described before [13–15].

Data selection and preparation for modelling. In each subject the highest quality RT3DE data set (Fig. 1A) was selected for

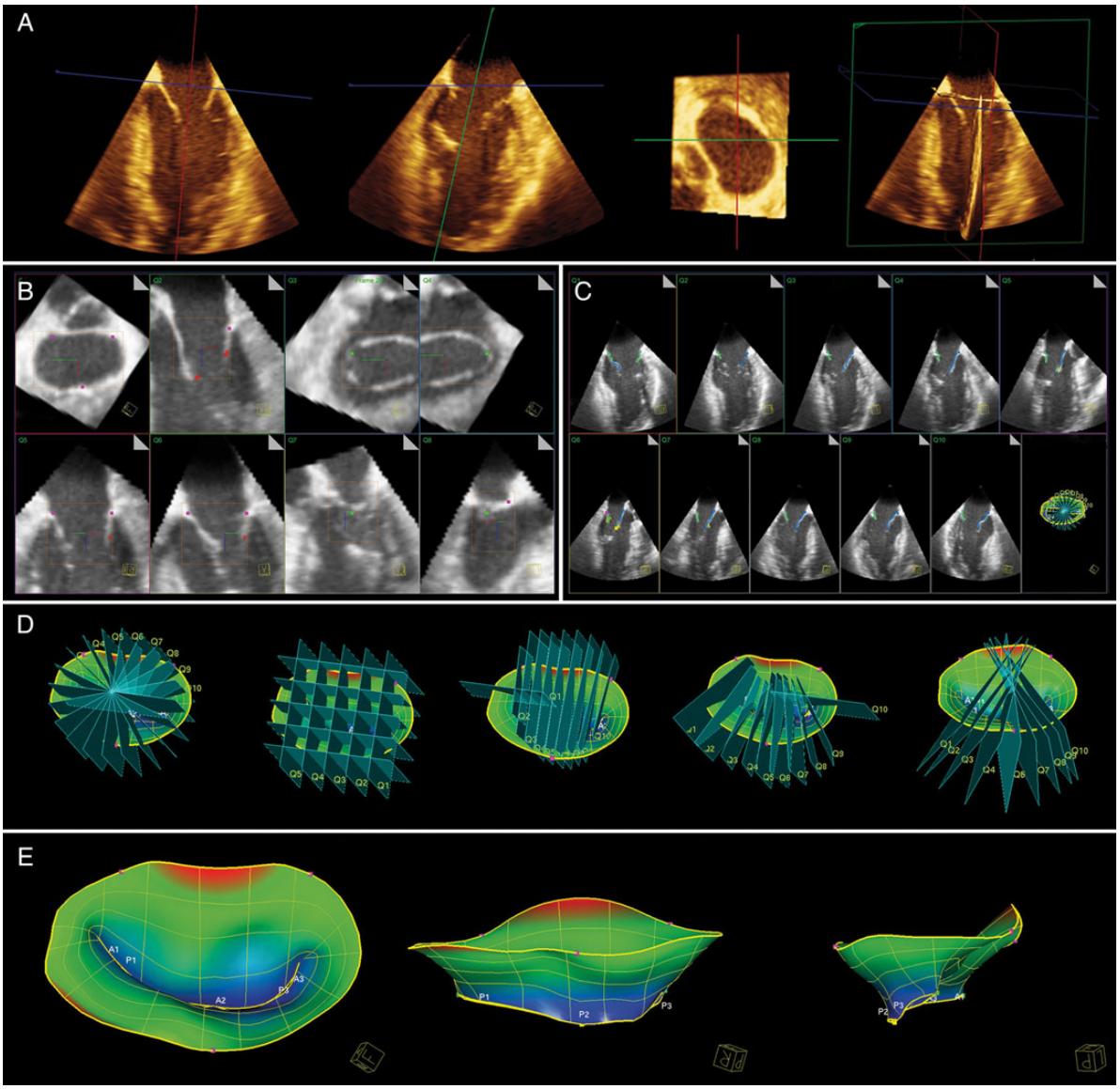

Figure 1: Technique for 4D modelling of the mitral valve (MV). (**A**) Full volume 3D transoesophageal data acquisition of the MV. (**B**) After import of real-time 3D echocardiography (RT3DE) data set into modeling software, automated representation in left atrial view, intercommissural view, long axis view, and full volume view followed by automated identification of landmarks of MV annulus and leaflets (magenta trigones, and center of posterior annulus, red leaflet tips, and green commissures) After visual verification of landmarks by the observer follows the automated identification of further landmarks of the MV annulus and leaflet tips (green: posterior leaflet; blue: anterior leaflet) (**C**) in 50 differently orientated planes (**D**). (**E**) After another visual inspection of the landmarks by the observer, automated modelling of the MV is based on the landmarks. This procedure is repeated semi-automatically for each frame of the cardiac cycle.

further analyses. Quality criteria were: highest frame rate, least stitching artefacts and complete depiction of all MV structures over the entire cardiac cycle. After importing the data into the software, the MV is presented in different views (Fig. 1B). Subsequently, the data set can be manually corrected with regard to the exact duration and end-points of the cardiac cycle, if indicated, using visual identification of end-systolic and end-diastolic frames. The end-systolic frame was defined as the last frame just before MV opening and the end-diastolic frame was defined the last frame just before aortic valve opening.

Landmark motion model. Initial recognition of the MV within the RT3DE data set was performed automatically by detection of seven major landmarks of the MV annulus and leaflets for each frame (Fig. 1B). The major landmarks are: the left trigone, the right trigone, the middle of the posterior annulus, the leaflet tips of the anterior and posterior leaflet in the plane between the middle of the posterior and anterior annulus, and the two commissures. In addition to these seven major landmarks, a total of 459 landmarks of the MV annulus are detected automatically in 50 differently orientated planes over each frame to depict detailed morphology of the MV (Fig. 1C and D). All landmarks can be corrected manually in each frame by the observer if indicated (e.g. stitching artefacts in the imported RT3DE data sets).

Comprehensive mitral model. A MV model was subsequently computed based on all aforementioned landmarks (Fig. 1E).

Quantification and 4D visualization. After visual verification of the accuracy of the surface model, the 4D MV model was displayed (Fig. 1E) with automatic quantification of MV morphology (Supplementary Figure I). With the presented model 39 different morphological parameters of the MV are currently issued over the entire cardiac cycle (Supplementary Table I). Measured data were exported for statistical analysis per frame and per percentage (from 0 to 90% in steps of 10%) of the cardiac cycle. Final MV model visualization was carried out per frame (Fig. 2) (Video 1).

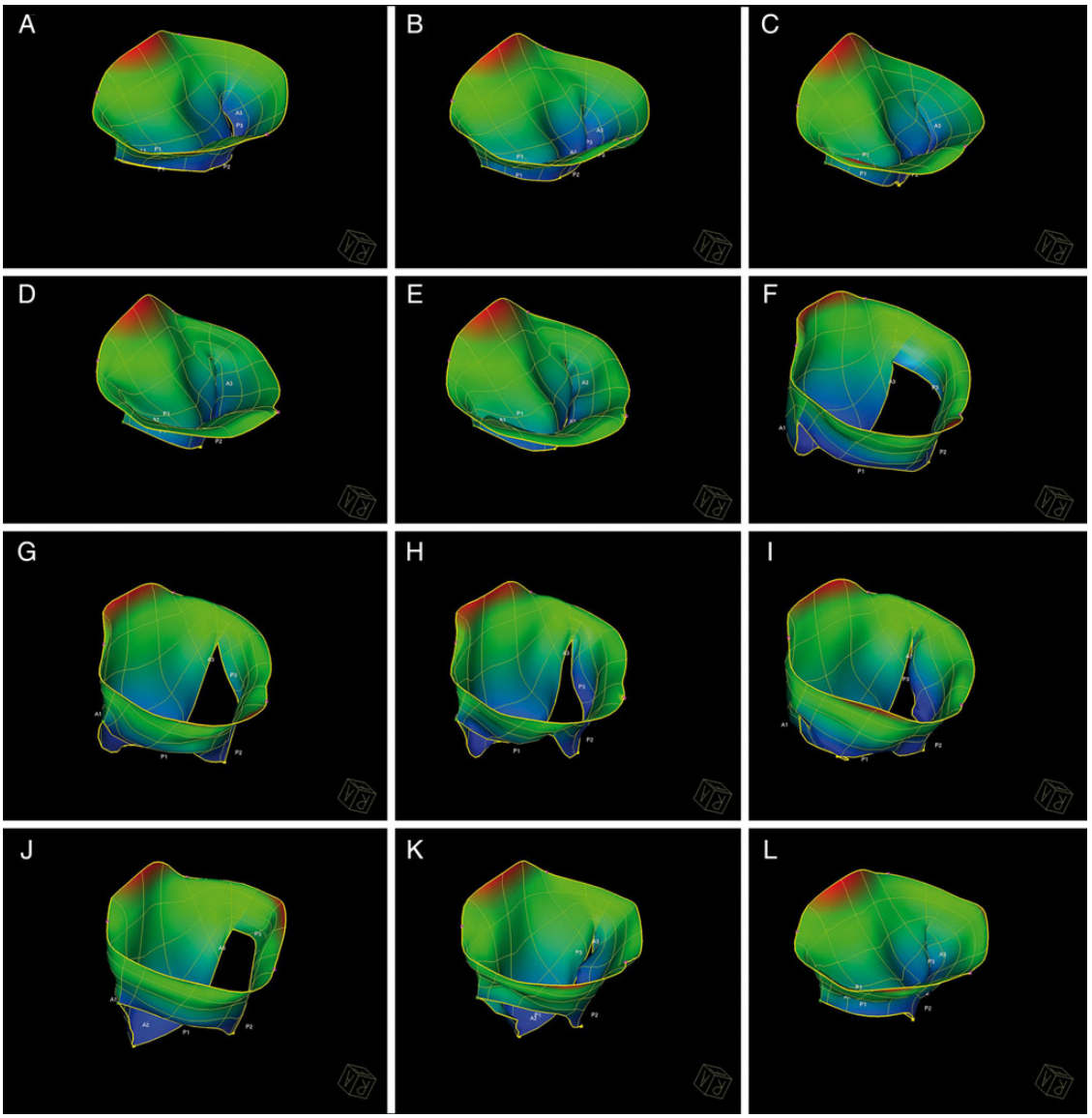

Figure 2: Four-dimensional visualization of mitral valve morphology for the entire cardiac cycle. (**A–E**) Systole an (**F–L**) diastole. The colour gradient shows the distance of the anatomical structure above (red) and below (blue) the annular level (green).

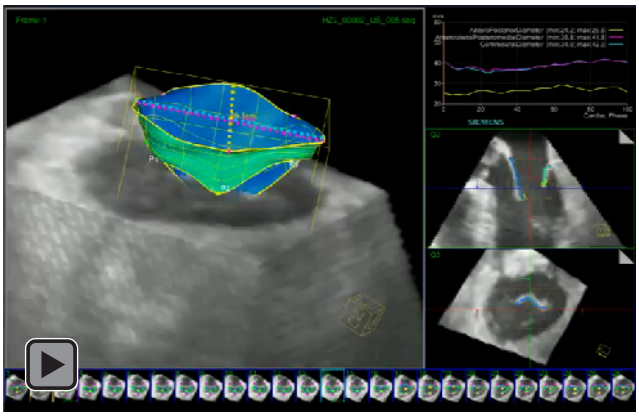

Video 1: Four-dimensional visualization and computed measurements of mitral valve morphology for the entire cardiac cycle.

Table 1: Patient characteristics

Variable	*n* = 18
Clinical	
Age (years)	68 ± 10
Women, *n* (%)	5 (28)
Body-mass index (kg/m^2)	30 ± 5
NYHA class, *n* (%)	
I	1 (5)
II	10 (56)
III/IV	7 (39)
CCS angina class, *n* (%)	
I	3 (17)
II	2 (11)
III	13 (72)
IV	0 (0)
Extent of coronary artery disease, *n* (%)	
One-vessel disease	0 (0)
Two-vessel disease	5 (28)
Three-vessel disease	13 (72)
Logistic EuroSCORE	6 ± 11
Echocardiography	
Left ventricular ejection fraction, %	54 ± 13
End-diastolic volume, ml	90 ± 36
End-systolic volume, ml	47 ± 36
Mitral regurgitation, *n* (%)	
Grad 0	14 (78)
Grad 1+	4 (22)

Data analysis

Proof of robustness and repeatability regarding interobserver and intraobserver comparison of the computed MV model was conducted selecting six key parameters. Specifically, MV annular geometry was described by the anteroposterior diameter, anterolateral–posteromedial diameter, annular area and annular circumference. Leaflet geometry was described by its intercommissural distance (distance between both commissures) and MV orifice area (area of valve orifice projected into its least square plane). All measurements were performed in mid-systole, end-systole, mid-diastole and end-diastole. The mid-systolic frame was defined as the middle frame between the end-diastolic frame and the end-systolic frame. The mid-diastolic frame was defined as the middle frame between the end-systolic frame and end-diastolic frame. Reproducibility of measurement was determined by repeating identical measurements

Table 2: Interobserver comparison of quantitative measurements over the entire cardiac cycle made by two observers in the population (*n* = 18)

Parameters	Mid-systole				End-systole				Mid-diastole				End-diastole			
	Observer 1 Mean ± SD	Observer 2 Mean ± SD	BIAS ± LOA	% Variability, Mean	Observer 1 Mean ± SD	Observer 2 Mean ± SD	BIAS ± LOA	% Variability, Mean	Observer 1 Mean ± SD	Observer 2 Mean ± SD	BIAS ± LOA	% Variability, Mean	Observer 1 Mean ± SD	Observer 2 Mean ± SD	BIAS ± LOA	% Variability, Mean
Anteroposterior diameter (mm)	27.3 ± 3.3	28.0 ± 3.0	−0.74 ± 1.63	2.7 ± 3.0	28.0 ± 3.6	28.6 ± 3.6	−0.56 ± 1.39	2.1 ± 2.5	27.5 ± 3.1	28.4 ± 3.1	−0.86 ± 2.55	3.1 ± 4.6	25.7 ± 3.1	26.6 ± 3.0	−0.90 ± 2.18	3.5 ± 4.3
Anterolateral–posteromedial diameter (mm)	35.8 ± 3.6	36.3 ± 3.3	−0.52 ± 1.72	1.5 ± 2.5	36.3 ± 3.8	36.4 ± 3.5	−0.18 ± 1.53	0.5 ± 2.1	37.7 ± 3.7	37.4 ± 3.7	−0.25 ± 1.20	0.7 ± 1.7	35.1 ± 3.3	35.6 ± 3.4	−0.44 ± 1.88	1.3 ± 2.7
Annular circumference (mm)	107.7 ± 9.9	111.0 ± 9.5	−3.38 ± 6.29	3.1 ± 2.9	108.7 ± 9.6	112.1 ± 9.8	−3.37 ± 5.12	3.1 ± 2.4	109.6 ± 9.4	112.3 ± 9.1	−2.70 ± 6.37	2.4 ± 2.9	104.8 ± 9.0	109.1 ± 9.6	−4.15 ± 8.37	3.9 ± 4.0
Mitral annular area (cm^2)	8.3 ± 1.5	8.6 ± 1.5	−0.29 ± 0.53	3.4 ± 3.2	8.5 ± 1.5	8.8 ± 1.6	−0.31 ± 0.49	3.6 ± 2.9	8.5 ± 1.3	8.8 ± 1.4	−0.24 ± 0.59	2.8 ± 3.4	7.7 ± 1.3	8.1 ± 1.4	−0.35 ± 0.66	4.5 ± 4.3
Intercommissural distance (mm)	24.3 ± 3.3[a]	27.0 ± 3.1[a]	−2.73 ± 5.82	10.7 ± 11.6	24.5 ± 3.3	26.6 ± 3.0	−2.16 ± 5.04	8.4 ± 10.1	29.4 ± 4.2	30.4 ± 3.8	−1.02 ± 3.55	3.4 ± 6.1	24.3 ± 5.0	26.6 ± 3.4	−2.32 ± 5.76	9.1 ± 11.6
Mitral valve area (cm^2)	0.2 ± 0.1	0.2 ± 0.1	0.00 ± 0.10	0.6 ± 0.2	0.2 ± 0.1	0.2 ± 0.1	0.02 ± 0.17	8.5 ± 41.5	2.6 ± 1.0	2.6 ± 1.0	−0.02 ± 0.33	0.7 ± 6.7	1.0 ± 1.2	1.0 ± 1.2	−0.01 ± 0.45	0.6 ± 23.8

[a]Student's paired *t*-test ($P = 0.02$).

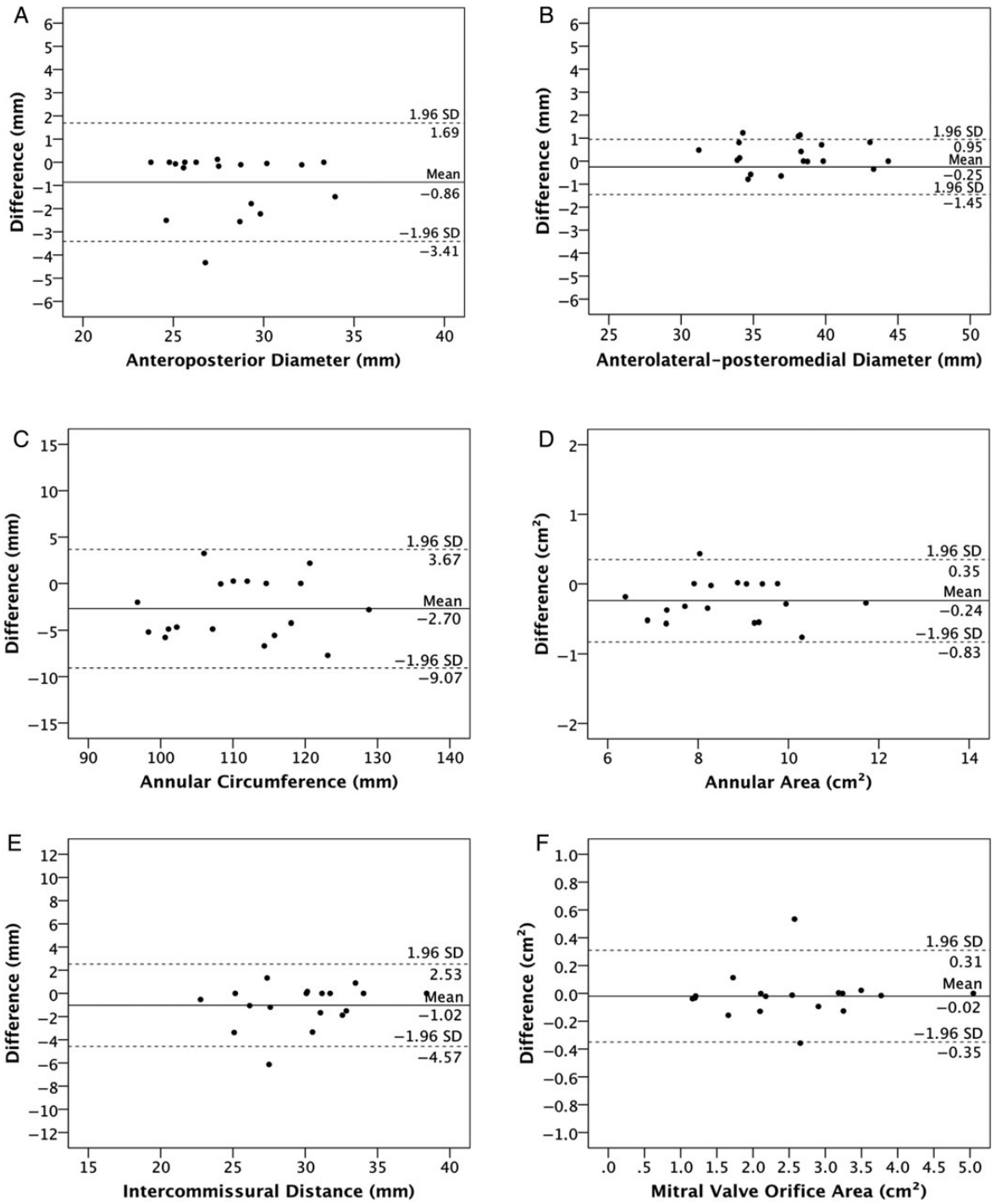

Figure 3: Representative Bland–Altman plots for interobserver comparison during mid-diastole. Analyses show the mean of observations (plotted along the *x*-axis) and differences between the measurements (plotted along the *y*-axis) of the two observers. Solid line indicates bias and dotted lines indicate two standard deviations above and below bias. All graphs for parameters in mid-diastole. Bland–Altman analysis for interobserver comparison for the entire cardiac cycle in Supplementary Figure I. (**A**) Anteroposterior diameter, (**B**) anterolateral–posteromedial diameter, (**C**) annular circumference, (**D**) mitral annular area, (**E**) intercommissural distance and (**F**) mitral valve orifice area.

on stored 3D data sets on 2 different days within 2 months by the same observer (intraobserver) and a different observer (interobserver).

Statistical analysis

All continuous data are presented as mean ± standard deviation (SD) and categorical data as percentage. Normal distribution of all continuous variables was confirmed with the Kolmogorov–Smirnov test. Student's paired *t*-test was used to evaluate for statistically significant difference between measurements. Interobserver and intraobserver variability were reported as bias±levels of agreement (LOA, 2 SD) as determined by Bland and Altman [16]. Reproducibility was assessed using the intraclass correlation coefficient (ICC) and Bland–Altman analysis. All analyses were performed using IBM SPSS Statistics Version 20 (IBM Deutschland

Table 3: Intraobserver comparison of quantitative measurements over the entire cardiac cycle made by two observers in the population (n = 18)

Parameters	Mid-systole				End-systole				Mid-diastole				End-diastole			
	Observer 1 Mean ± SD	Observer 2 Mean ± SD	BIAS ± LOA	% Variability, Mean	Observer 1 Mean ± SD	Observer 2 Mean ± SD	BIAS ± LOA	% Variability, Mean	Observer 1 Mean ± SD	Observer 2 Mean ± SD	BIAS ± LOA	% Variability, Mean	Observer 1 Mean ± SD	Observer 2 Mean ± SD	BIAS ± LOA	% Variability, Mean
Anteroposterior diameter (mm)	27.3 ± 3.3	27.1 ± 3.2	0.14 ± 2.14	0.5 ± 4.0	28.0 ± 3.6	27.6 ± 3.3	0.45 ± 1.80	1.6 ± 3.3	27.5 ± 3.1	27.3 ± 2.9	0.29 ± 2.10	1.1 ± 3.9	25.7 ± 7.1	25.5 ± 3.0	0.18 ± 2.29	0.7 ± 5.6
Anterolateral–posteromedial diameter (mm)	33.3 ± 11.1	34.0 ± 11.2	−0.71 ± 2.39	2.0 ± 3.4	36.3 ± 3.8	36.7 ± 3.7	−0.46 ± 1.82	1.1 ± 2.2	37.7 ± 3.7	38.0 ± 3.8	−0.31 ± 1.45	0.8 ± 2.0	35.1 ± 3.3	35.6 ± 3.2	−0.51 ± 1.61	1.4 ± 2.2
Annular circumference (mm)	107.7 ± 9.9	106.1 ± 9.1	1.54 ± 7.23	1.4 ± 3.5	108.7 ± 9.6	107.4 ± 9.5	1.35 ± 7.47	1.2 ± 3.5	109.6 ± 9.4	108.3 ± 8.7	1.29 ± 6.88	1.2 ± 3.2	104.9 ± 9.0	104.1 ± 7.6	−3.39 ± 9.06	3.3 ± 4.4
Mitral annular area (cm^2)	8.3 ± 1.5	8.1 ± 1.4	0.19 ± 0.65	2.3 ± 4.0	8.5 ± 1.5	8.3 ± 1.5	0.15 ± 0.71	1.8 ± 4.3	8.5 ± 1.3	8.4 ± 1.3	0.16 ± 0.71	1.9 ± 4.3	7.7 ± 1.3	7.6 ± 1.2	0.08 ± 0.82	1.1 ± 5.5
Intercommissural distance (mm)	24.3 ± 3.3	24.5 ± 2.5	−0.22 ± 5.27	0.9 ± 11.0	24.5 ± 3.3	25.2 ± 2.1	−0.75 ± 4.92	3.0 ± 10.1	29.4 ± 4.2	28.7 ± 3.8	0.64 ± 4.63	2.2 ± 8.1	24.3 ± 5.0	25.0 ± 3.4	−0.70 ± 5.92	2.8 ± 12.2
Mitral valve area (cm^2)	0.2 ± 0.1	0.2 ± 0.2	−0.04 ± 0.31	22.4 ± 83.1	0.2 ± 0.1	0.3 ± 0.2	−0.04 ± 0.33	16.9 ± 71.1	2.6 ± 1.0	2.6 ± 1.0	−0.02 ± 0.19	0.7 ± 4.0	1.0 ± 1.2	0.9 ± 1.2	0.02 ± 0.49	2.1 ± 26.2

GmbH, Ehningen). A probability value of <0.05 was considered statistically significant.

RESULTS

Patient characteristics and procedural data

Eighteen patients (mean age 68 ± 10 years; 13 males) underwent standard coronary bypass graft surgery. The mean left ventricular ejection fraction was 54 ± 13% (Table 1). The majority of patients (72%) had three-vessel coronary artery disease. The MV was completely normal in 14 patients (78%). Mild MR was present in 4 patients (22%). Three ECG-gated transoesophageal echocardiography data sets for each patient were obtained and recorded. Image segmentation and MV modelling for each patient were accomplished in <2 min. Manual correction of landmarks was needed.

Interobserver comparison

There were non-significant differences between the two observers for all measurements (P range, 0.05–0.99) except the mid-systolic intercommissural distance (bias + LOA, −2.73 ± 5.82; P = 0.02) (Table 2). Bland–Altman analysis plots for interobserver comparison in mid-systole and mid-diastole showed a random scatter of points around 0, indicating no systematic bias or no measurement error proportional to the measurement value (Fig. 3). Supplementary Figure II show all 24 Bland–Altman analysis plots for all quantitative measurements during mid-systole, end-systole, mid-diastole and end-diastole.

The lowest variability over the cardiac cycle was seen for the anterolateral–posteromedial diameter (range, 0.5–1.5%), whereas the intercommissural distance showed the highest variability (range, 3.4–10.7%) (Table 2).

Reproducibility is described for anteroposterior diameter, anterolateral–posteriomedial diameter, annular circumference and mitral annular area (ICC range, 0.895–0.987) (Table 4) . The ICC for MV orifice area was acceptable at end-systole (0.756), and excellent in all other cardiac phases (range, 0.915–0.986). The ICC for intercommissural distance was acceptable in diastolic phases (range, 0.763–0.896), and reasonable in systolic phases (range, 0.571–0.661). These results depict a lower reproducibility in all systolic phases for intercommissural distance.

Intraobserver comparison

There were no statistically significant differences between the two observations by one observer (P range, 0.42–0.96) (Table 3). Bland–Altman analysis plots for intraobserver comparison in mid-systole and mid-diastole showed no systematic bias or measurement error proportional to the measurement value (Fig. 4). Supplementary Figure III shows all 24 Bland–Altman analysis plots for all quantitative measurements during mid-systole, end-systole, mid-diastole and end-diastole.

The lowest variability over the cardiac cycle was seen in the anteroposterior diameter (range, 0.5–1.6%), whereas the MV orifice area showed the highest variability (range, 0.7–22.4%) (Table 3).

The ICC was excellent over the entire cardiac cycle for anteroposterior diameter, anterolateral–posteromedial diameter, annular

Table 4: Intraclass correlation coefficients for interobserver and intraobserver analysis for each mitral valve parameter

Parameters	Mid-systole		End-systole		Mid-diastole		End-diastole	
	Interobserver	Intraobserver	Interobserver	Intraobserver	Interobserver	Intraobserver	Interobserver	Intraobserver
Anteroposterior diameter (mm)	0.966	0.945	0.980	0.965	0.912	0.936	0.933	0.926
Anterolateral–posteromedial diameter (mm)	0.967	0.940	0.977	0.969	0.986	0.980	0.959	0.969
Annular circumference (mm)	0.945	0.925	0.964	0.921	0.939	0.925	0.895	0.827
Mitral annular area (cm^2)	0.984	0.975	0.987	0.972	0.976	0.962	0.967	0.942
Intercommissural distance (mm)	0.571	0.582	0.661	0.585	0.896	0.824	0.763	0.750
Mitral valve area (cm^2)	0.915	0.446*	0.756	0.539	0.986	0.995	0.981	0.977

All P for ICC <0.01, except *P = 0.03.

circumference and mitral annular area (range, 0.827–0.980) (Table 4). For MV orifice area, the ICC was reasonable in all systolic phases (range, 0.446–0.539), and excellent in all diastolic phases (range, 0.977–0.995). For intercommissural distances, the ICC was acceptable in all diastolic phases (range, 0.750–0.824), and reasonable in all systolic phases (range, 0.582–0.585).

DISCUSSION

This newly developed RT3DE-based semi-automated 4D MV model enables pre-eminent quantitative analysis of the MV morphology and structure. Feasibility, reliability and reproducibility of patient-specific quantification of the MV geometry over the entire cardiac cycle are proved herein. MV 4D visualization and quantification result in a spatial resolution not achieved thus far.

4D reconstruction of mitral valve

RT3DE analysis of the MV apparatus, generally considered a highly complex structure, is gaining importance while contributing to the understanding of MV function, especially when considering the well-known limitations of 2D echocardiography (2DE) [5–7]. It is obvious that 'mental reconstruction' based on separate 2D MV images does not provide comparable 'intuitive' information compared with 3D reconstruction [12]. Thus, the accuracy of 2DE examinations especially for more complex MV pathologies has significant limitations [17–19]. RT3DE imaging modalities display consecutive dynamic 3D images of the MV with subsequent analysis of each individual component of the MV [20].

Specified software for 3D modelling of the MV based on RT3DE data has been developed to precisely quantify the MV [3–5, 14, 21]. As previously described, the duration needed for 3D MV quantification at any selected time during the cardiac cycle (e.g. mid-diastole) varies between 5 min and 4 h [4, 5, 22]. Adding a timeline (cardiac cycle) to 3D reconstruction, a so-called 4D reconstruction of the MV can be realized, which represents an extension with a not yet defined potential for analysis of MV morphology and function. In addition, the model presented herein is to the best of our knowledge the first model to perform complete cardiac cycle 3D analysis of the complete MV apparatus in <5 min including the opportunity for visual inspection and manual correction of MV landmarks if indicated. The model also allows for detailed quantification of even very small morphological changes of any MV component over the complete cardiac cycle. This is accomplished using a learning pattern-based algorithm with subsequent integration in 4D reconstructions within a Cartesian coordinate system. In addition to pre-eminent motion pictures of the MV, this allows up to 39 different geometric measurements at any point of time of the cardiac cycle [13, 14].

It is very likely that, due to the significantly reduced time consumption and excellent low levels of variability for this model, this technology has a high chance for rapid integration into clinical practice.

The only exception to the high reproducibility was the measurement of leaflet variables (intercommissural distance, MV orifice area) during systole (variability range: 8–22%). The reason for this is that the determination of the exact commissural distance between the anterolateral and posteromedial commissure is very difficult in the closed state of the MV. It is widely accepted that the anterolateral and posteromedial commissures are not exact anatomical landmarks, but rather commissural leaflets. The commissural leaflets provide continuity between the anterior and posterior leaflet and consist of several millimetres of tissue. Owing to the small clefts of the commissural leaflets, both observers have interpreted the end of the commissure differently. In contrast to systole, the intercommissural distance in mid-diastole showed a low variability (range: 2–3%). In end-diastole, there was a decline in variability (range: 3–9%). This can be explained by the fact that, in many cases, the MV was almost closed. Thus, the value of the intercommissural distance during the closed state of the MV must be critically evaluated. Mitral valve area also showed increased variability during systole. This is explained by the low values of 0.2 cm^2. Through the round of measured values arise at low values, a high error-including high variability. These are the measurements that very accurately show the low variability during diastole.

Limitations

The presented method has limitations, which are outlined below. (i) The model is based on RT3DE data sets. Accordingly, the limitations of RT3DE also apply for our technology. These have been well described before [5]. One important limitation is that the RT3DE data set requires R-wave gating. Also, the image reconstruction is based on the principle of stitching together multiple cut planes over four cardiac cycles. Therefore, the measurement results of the 4D MV model are also composed of four different

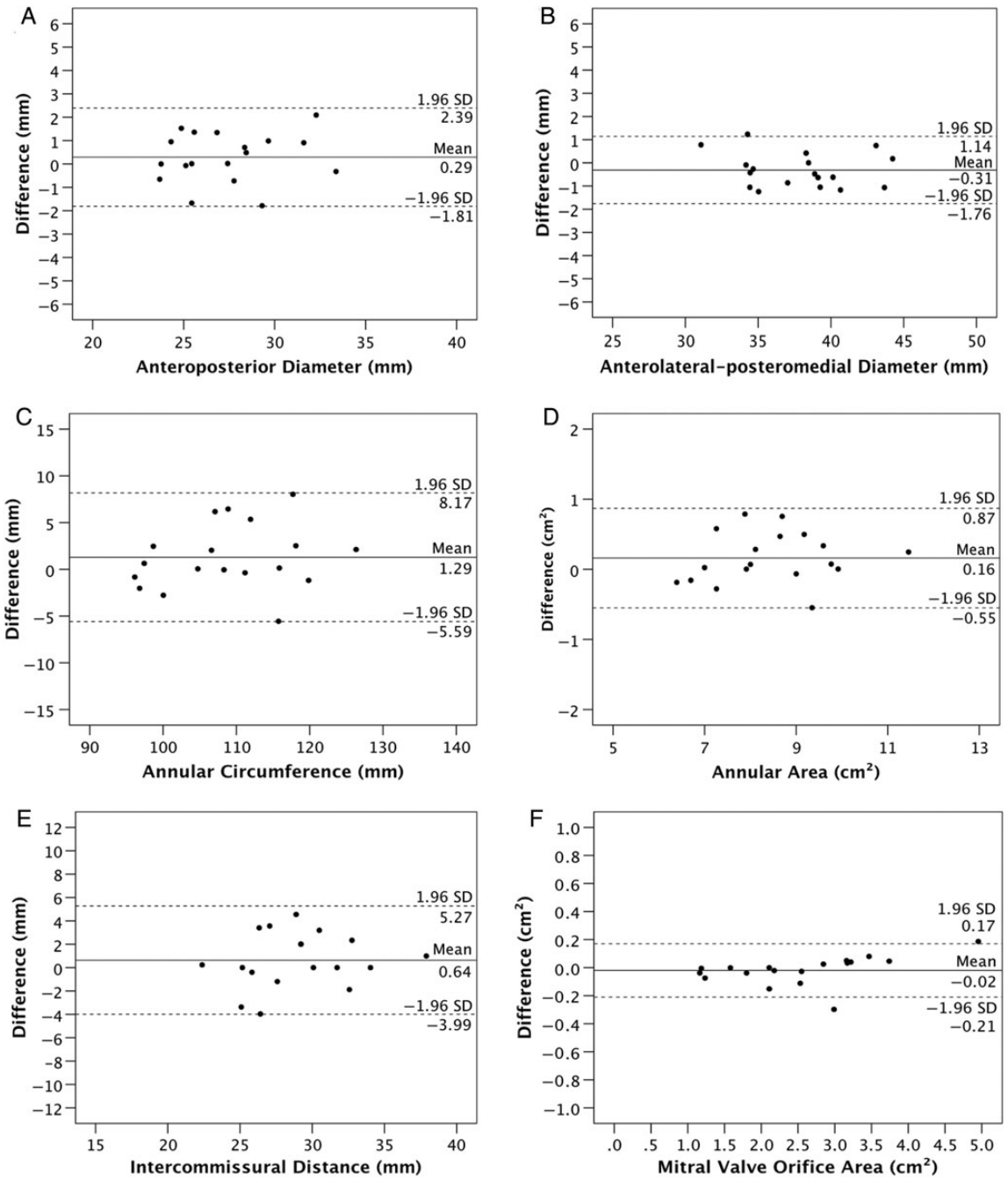

Figure 4: Representative Bland–Altman plots for intraobserver comparison during mid-diastole. Analyses show the mean of observations (plotted along the *x*-axis) and differences between the measurements (plotted along the *y*-axis) of the two observations. Solid line indicates bias and dotted lines indicate two standard deviations above and below bias. All graphs for parameters in mid-diastole. Bland–Altman analysis for intraobserver comparison for the entire cardiac cycle in Supplementary Figure II. (**A**) Anteroposterior diameter, (**B**) anterolateral–posteromedial diameter, (**C**) annular circumference, (**D**) mitral annular area, (**E**) intercommissural distance and (**F**) mitral valve orifice area.

cardiac cycles. Furthermore, (ii) in our experience, suitable RT3DE data sets with less than 8 frames per cardiac cycle were strictly limited for 4D reconstruction. In these cases, a detailed temporal allocation to the individual cardiac phases was difficult. Therefore, a high sampling rate and high data quality during data acquisition must be accomplished. (iii) Patient-specific severe calcification of the mitral annulus or complex MV morphology with billowing and high number of clefts in the RT3DE data sets required more time for MV modelling. Reasons for this are time-consuming visual inspections and manual corrections of landmarks. Despite the time-consuming 4D reconstruction, precise quantifications of the MV were possible. (iv) Finally, we have not compared our measurements with independent standards, such as measurement during surgery. The measurements reported here are consistent with previously reported values for the mitral annulus [4, 23]. The accuracy of automated measurements compared with measurements made during surgery needs to be tested in future studies.

CONCLUSION

This newly developed RT3DE-based 4D MV model demonstrates rapid excellent morphological visualization and comprehensive quantification of the MV apparatus with high levels of reliability and reproducibility yet to be reported.

SUPPLEMENTARY MATERIAL

Supplementary material is available at *ICVTS* online.

Conflict of interest: Joerg Seeburger and Friedrich Wilhelm Mohr received research support from Siemens AG. Razvan Ioan Ionasec and Ingmar Voigt are employees of Siemens AG.

Funding

This work was supported by the Heart Center Leipzig University and ProCordis – Verein zur Förderung der Forschung in der Herzchirurgie e.V.

REFERENCES

[1] Van Mieghem NM, Piazza N, Anderson RH, Tzikas A, Nieman K, De Laat LE *et al*. Anatomy of the mitral valvular complex and its implications for transcatheter interventions for mitral regurgitation. J Am Coll Cardiol 2010;56:617–26.
[2] Muresian H. The clinical anatomy of the mitral valve. Clin Anat 2009;22:85–98.
[3] Calleja A, Thavendiranathan P, Ionasec RI, Houle H, Liu S, Voigt I *et al*. Automated quantitative 3-dimensional modeling of the aortic valve and root by 3-dimensional transesophageal echocardiography in normals, aortic regurgitation, and aortic stenosis: comparison to computed tomography in normals and clinical implications. Circ Cardiovasc Imaging 2013;6:99–108.
[4] Jassar AS, Brinster CJ, Vergnat M, Robb JD, Eperjesi TJ, Pouch AM *et al*. Quantitative mitral valve modeling using real-time three-dimensional echocardiography: technique and repeatability. Ann Thorac Surg 2011;91:165–71.
[5] Mahmood F, Karthik S, Subramaniam B, Panzica PJ, Mitchell J, Lerner AB *et al*. Intraoperative application of geometric three-dimensional mitral valve assessment package: a feasibility study. J Cardiothorac Vasc Anesth 2008;22:292–8.
[6] Altiok E, Hamada S, Brehmer K, Kuhr K, Reith S, Becker M *et al*. Analysis of procedural effects of percutaneous edge-to-edge mitral valve repair by 2D and 3D echocardiography. Circ Cardiovasc Imaging 2012;5:748–55.
[7] Lee AP, Hsiung MC, Salgo IS, Fang F, Xie JM, Zhang YC *et al*. Quantitative analysis of mitral valve morphology in mitral valve prolapse with real-time 3-dimensional echocardiography: importance of annular saddle shape in the pathogenesis of mitral regurgitation. Circulation 2013;127:832–41.
[8] Vergnat M, Jassar AS, Jackson BM, Ryan LP, Eperjesi TJ, Pouch AM *et al*. Ischemic mitral regurgitation: a quantitative three-dimensional echocardiographic analysis. Ann Thorac Surg 2011;91:157–64.
[9] Vergnat M, Levack MM, Jassar AS, Jackson BM, Acker MA, Woo YJ *et al*. The influence of saddle-shaped annuloplasty on leaflet curvature in patients with ischaemic mitral regurgitation. Eur J Cardiothorac Surg 2012;42:493–9.
[10] Vergnat M, Levack MM, Jackson BM, Bavaria JE, Herrmann HC, Cheung AT *et al*. The effect of surgical and transcatheter aortic valve replacement on mitral annular anatomy. Ann Thorac Surg 2013;95:614–9.
[11] Chandra S, Salgo IS, Sugeng L, Weinert L, Tsang W, Takeuchi M *et al*. Characterization of degenerative mitral valve disease using morphologic analysis of real-time three-dimensional echocardiographic images: objective insight into complexity and planning of mitral valve repair. Circ Cardiovasc Imaging 2011;4:24–32.
[12] Lang RM, Badano LP, Tsang W, Adams DH, Agricola E, Buck T *et al*. EAE/ASE recommendations for image acquisition and display using three-dimensional echocardiography. Eur Heart J Cardiovasc Imaging 2012;13:1–46.
[13] Ionasec RI, Voigt I, Georgescu B, Wang Y, Houle H, Hornegger J *et al*. Personalized modeling and assessment of the aortic-mitral coupling from 4D TEE and CT. Med Image Comput Comput Assist Interv 2009;12:767–75.
[14] Ionasec RI, Voigt I, Georgescu B, Wang Y, Houle H, Vega-Higuera F *et al*. Patient-specific modeling and quantification of the aortic and mitral valves from 4-D cardiac CT and TEE. IEEE Trans Med Imaging 2010;29:1636–51.
[15] Noack T, Kiefer P, Ionasec R, Voigt I, Mansi T, Vollroth M *et al*. New concepts for mitral valve imaging. Ann Cardiothorac Surg 2013;2:787–95.
[16] Bland JM, Altman DG. Statistical methods for assessing agreement between two methods of clinical measurement. Lancet 1986;1:307–10.
[17] Grewal KS, Malkowski MJ, Kramer CM, Dianzumba S, Reichek N. Multiplane transesophageal echocardiographic identification of the involved scallop in patients with flail mitral valve leaflet: intraoperative correlation. J Am Soc Echocardiogr 1998;11:966–71.
[18] Stewart WJ, Currie PJ, Salcedo EE, Klein AL, Marwick T, Agler DA *et al*. Evaluation of mitral leaflet motion by echocardiography and jet direction by Doppler color flow mapping to determine the mechanisms of mitral regurgitation. J Am Coll Cardiol 1992;20:1353–61.
[19] Mahmood F, Subramaniam B, Gorman JH III, Levine RM, Gorman RC, Maslow A *et al*. Three-dimensional echocardiographic assessment of changes in mitral valve geometry after valve repair. Ann Thorac Surg 2009;88:1838–44.
[20] Lancellotti P, Moura L, Pierard LA, Agricola E, Popescu BA, Tribouilloy C *et al*. European Association of Echocardiography recommendations for the assessment of valvular regurgitation. Part 2: mitral and tricuspid regurgitation (native valve disease). Eur J Echocardiogr 2010;11:307–32.
[21] Veronesi F, Corsi C, Sugeng L, Mor-Avi V, Caiani EG, Weinert L *et al*. A study of functional anatomy of aortic-mitral valve coupling using 3D matrix transesophageal echocardiography. Circ Cardiovasc Imaging 2009;2:24–31.
[22] Hozumi T, Yoshikawa J. Three-dimensional echocardiography using a muliplane transesophageal probe: the clinical applications. Echocardiography 2000;17:757–64.
[23] Grewal J, Suri R, Mankad S, Tanaka A, Mahoney DW, Schaff HV *et al*. Mitral annular dynamics in myxomatous valve disease: new insights with real-time 3-dimensional echocardiography. Circulation 2010;121:1423–31.